ISSN 8755-6839

SCIENCE OF **TSUNAMI HAZARDS**

Journal of Tsunami Society International

Volume 41 **Number 1** **2022**

EFFECTIVE TSUNAMI EARLY WARNING USING THE PRODUCT OF P-WAVE DOMINANT PERIOD AND SOURCE RUPTURE DURATION OF MORE THAN 50 SECONDS

Madlazim[1], Tjipto Prastowo[1], Muhammad Nurul Fahmi[1], Ella Melianda[2], Soerja Kusuma[3]

[1]Universitas Negeri Surabaya, Surabaya 60231, Indonesia. E-mail: madlazim@unesa.ac.id
[2]Universitas Syiah Kuala, Aceh, Indonesia
[3]Universitas Sebelas Maret, Surakarta, Indonesia

ABSTRACT

In this study, we used a tsunami-faulting model, where the discriminant for tsunami potential is the dominant period T_d of *P*-waves times the rupture duration of an earthquake T_{50ex} of more than 50 seconds. The product of T_dT_{50ex} was estimated in real time and validated with Tsunami Event Validity (TEV) from NOAA/WDC database. The T_dT_{50ex} discriminant was calculated using a direct procedure for the vertical component of *P*-wave seismograms velocity. The data were obtained from 51 earthquakes that occurred during 2011-2020 with magnitudes of $6.5 \leq M_w \leq 8.6$, containing 19 strike-slips fault, 11 normal-fault and 21 reverse-fault earthquakes. The results suggest that earthquakes are said to be potential to generate tsunamis when $T_dT_{50ex} \geq 10$ s is satisfied. In summary, T_dT_{50ex} is proved to be an efective tsunami discriminant to detect the presence of a tsunami wave after about 4 minutes an earthquake occurs, implying that this is (can be accessed at http://prediksi-tsunami.unesa.ac.id/www/index.html) a useful parameter for rapid and accurate tsunami early warning.

Keywords: *Tsunami early warning; P-wave dominant period; Source rupture duration more than 50 s; product of T_dT_{50ex}; efective tsunami discriminant.*

1. INTRODUCTION

There are currently two earthquake rupture models used for tsunami early warning. The first model is a seismic-faulting model and the second one is a tsunami-faulting model. The former is related to tsunami potential that depends on seafloor displacement. This displacement is related to the length L, width W, mean slip D, and depth z of earthquake rupture. The main discriminant used in this model for tsunami generation is the centroid-moment tensor magnitude $M_{\mathrm{w}}^{\mathrm{CMT}}$ reflecting the LWD product and is indirectly estimated using an inversion procedure (Polet & Kanamori, 2009). However, $M_{\mathrm{w}}^{\mathrm{CMT}}$ values depend on rupture depth, earth model, seismic instrument, and is only available 20-30 minutes or longer after an earthquake occurs (Lomax & Michelini, 2012). The tsunami model is particularly related to the length L and width W of the rupture. Two tsunami parameters for this model are rupture duration of more than 50 seconds $T_{50\mathrm{ex}}$, representing the length L of the rupture and P-wave dominant period T_{d}, representing the width W of the rupture. The values of T_{d} and $T_{50\mathrm{ex}}$ can be determined using direct procedures from P-wave seismograms on vertical velocity records. For near-field events, it only takes no more than 4 minutes to complete calculation (Madlazim et al., 2019).

Effective tsunami early warning is early warning that can communicate tsunami potential from an earthquake quickly and accurately so that people potentially affected by a tsunami have time to save their lives. Tsunamis are particularly most devastating in effects at distances less than 1000 km from the epicenter and may arrive within 20-30 minutes after the event origin time (OT). It follows that tsunami alert at these distances requires quick and accurate notification within 15 minutes or less after OT for effective early warning (Tsushima et al., 2011; Newman et al., 2011; Sutton et al., 2018). Currently, there have been many organizations that use the seismic model for rapid assessment of tsunami excitation, including the Indonesian Agency for Geophysics, Climatology, and Meteorology (BMKG), the Japan Meteorological Agency (JMA), the German-Indonesian Tsunami Early Warning System (GITEWS) and the Pacific Tsunami Warning Centre (PTWC). Lomax and Michelini (2011; 2012) argued that this model depends particularly on the initial estimates of earthquake epicenter, depth, seismic moment M_{o} and moment magnitude M_{w} or other equivalent magnitude scales.

Knowledge of seismic moment M_{o} is important for tsunami early warning because tsunami potential by a shallow, underwater earthquake depends on seabed displacement, which can be linked to the seismic potency represented by the LWD product. Since $M_{\mathrm{o}} = \mu LWD$, where μ is the shear at the source, then the seismic potency and hence tsunami potential must be scaled with $LWD = M_{\mathrm{o}}/\mu$ (Lomax and Michelini, 2011; 2012). On the other hand, M_{w} is a good discriminant for tsunami potential but it does not hold for all events having the potency for tsunami generation. In particular, the M_{w} discriminant does not work for slow 'tsunami earthquakes', which induce waves larger than would be expected from their sizes (Satake, 2002; Polet and Kanamori, 2009; Newman et al., 2011; Lomax and Michelini, 2012).

To avoid these problems, namely the lack of speed and accuracy in effective tsunami early warning, especially for near to regional distances, we recommend the use of the tsunami model, where the $T_{\mathrm{d}}T_{50\mathrm{ex}}$ discriminant is obtained quicker and more accurate for assessment of tsunami potential. A direct procedure for assessing possible tsunami generation caused by earthquakes was discussed by Lomax and Michelini (2009; 2011) and Madlazim et al. (2011; 2013; 2015; 2019). For large earthquakes, the $T_{\mathrm{d}}T_{50\mathrm{ex}}$ product increases as rupture depth decreases due to shear modulus

effects and reduction in rupture velocity (Lomax and Michelini, 2012). This suggests that the T_dT_{50ex} discriminant provides more information on tsunami impact than M_w^{CMT} and other discriminants do for tsunami early warning (Lomax and Michelini, 2011; 2012; Madlazim et al., 2019). This implies that the potency for tsunami generation after an earthquake occurs is not directly related to the *LWD* product derived from the seismic model (Lomax and Michelini, 2011; 2012).

Tsunami potential is well constrained by information about the length and depth of rupture, where such information is provided by the product of T_dT_{50ex}. It follows that estimates of the rupture length and depth that are difficult and impossible to obtain quickly are not required. This reflects that the T_dT_{50ex} value is found to represent a good tsunami discriminant derived from the tsunami model that corresponds to the observed tsunami waves (Satake, 1994; Lomax and Michelini, 2012; Lay et al., 2017). In this study, we show that using the vertical velocity records of the *P*-wave seismograms in our real-time application for tsunami assessment and its corresponding prediction, accessed at http://prediksi-tsunami.unesa.ac.id/www/index.html, the T_dT_{50ex} calculation can then be completed in less than 4 minutes after the OT for short-range earthquakes.

METHODS

We used direct procedures of calculation for relatively quick assessment of tsunami generation using a tsunami discriminant, namely T_dT_{50ex}. This discriminant is the product of the *P*-wave dominant period T_d and the rupture duration T_{50ex} longer than 50 s from the vertical velocity records on the high-frequency, *P*-wave seismograms.

1. The measurement of *P*-wave dominant period T_d

We used definition of the dominant period T_d for an event as the median of the dominant period values for each station given by the peak of the τ_c algorithm (Nakamura, 1988; Wu and Kanamori, 2005; Lomax and Michelini, 2011) applied with a 5 s sliding time-window from 0 to 55 s after the *P*-wave arrival on velocity seismograms (Eq. 1). The T_d estimation was performed using a direct procedure with no inversion, making the calculation process relatively short. The first step of the T_d estimation was to determine time domain τ_c as follows:

$$\tau_c = 2\pi \int_{T_2}^{T_1} v^2(t)dt \Big/ \int_{T_2}^{T_1} \acute{v}^2(t)dt \qquad (1)$$

where $T_1 = 0$ (the onset time of *P*-waves) and $T_2 = 55$ s acquired from regional data. Detailed steps of the T_d estimation are as follows: (1) preparing raw earthquake velocity records from the vertical component of broadband seismograms in a miniseed format; (2) applying 4-poles and a corner frequency of 0.05 Hz Butterworth bandpass filter, the vertical component of velocity records for each station; (3) picking *P*-wave arrival times automatically for the vertical component of velocity seismograms; (4) integrating the seismograms and comparing them with the vertical acceleration of broadband seismograms times 2π of arrival times of *P*-waves automatically picked up from the vertical velocity records on the seismograms; and (5) taking the final results as values of the dominant period T_d, the maximum value in time domain (see Fig. 1, second panel).

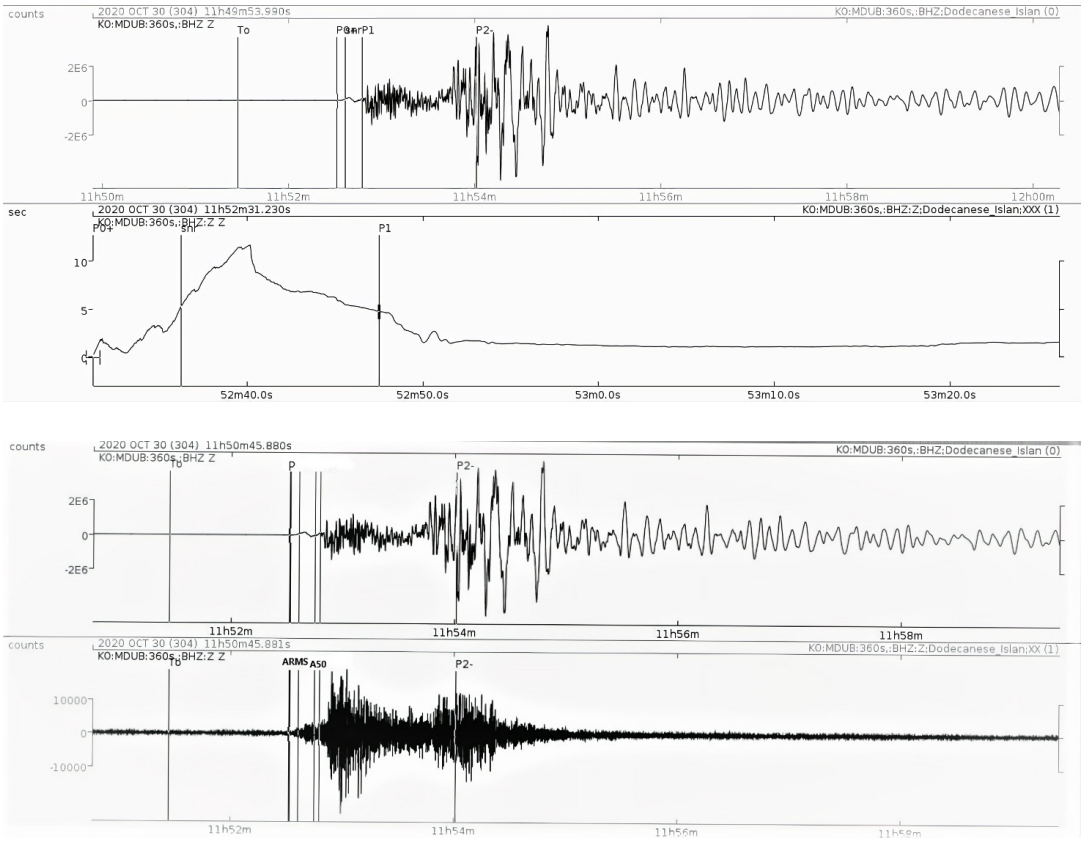

Figure 1. Schematic of a single-station, $T_{\mathrm{d}}T_{50\mathrm{ex}}$ processing for the 2020.10.30, M_{w} 7.0, Dodecanese Island, Greece earthquake recorded by station KO.MDUP at 4.26° GCD. Top panel represents raw, broadband velocity and the second panel shows T_{d} estimate. The third panel is raw and bottom panel is HF seismogram, showing an estimate of $T_{50\mathrm{ex}} = A_{50}/A_{\mathrm{RMS}}$.

2. The measurement of rupture duration $T_{50\mathrm{ex}}$ longer than 50s

Earthquake rupture duration $T_{50\mathrm{ex}}$ longer than 50 s is a substitute for rupture duration (Lomax and Michelini, 2011). For estimates of the rupture duration longer than 50s, $T_{50\mathrm{ex}}$ were performed using a direct procedure with no inversion, making the calculation process relatively shortened. The first step of $T_{50\mathrm{ex}}$ estimates was determined according to Lomax and Michelini (2011) and Madlazim (2013) as follows:

$$T_{50\mathrm{ex}} = A_{50}/A_{\mathrm{RMS}} \qquad (2)$$

where A_{50} is the average amplitude for 50 until 60 seconds and A_{RMS} is the average amplitude for 0 until 25 seconds.

The followings are detailed steps of determining the $T_{50\mathrm{ex}}$ exceeding 50 s using a direct procedure: (1) preparing raw data from the vertical component of broadband seismograms in a miniseed format; (2) applying 4-poles and the 5-20 Hz Butterworth bandpass filter to obtain the high-frequency, vertical component of seismic velocity records for each station; (3) picking arrival

times of *P*-waves automatically at the high-frequency, vertical velocity seismograms; (4) calculating the RMS amplitude and A_{50} values; and (5) estimating T_{50ex} using the ratio of A_{50} to the RMS amplitude values (see Fig. 1, bottom panel). Figure 1 describes Schematic of a single-station, T_dT_{50ex} processing for the 2020.10.30, M_w 7.0, Dodecanese Island, Greece earthquake recorded by station KO.MDUP at 4.26° GCD. Top panel represents raw, broadband velocity and the second panel shows T_d estimate. The third panel is raw and bottom panel is HF seismogram, showing an estimate of $T_{50ex} = A_{50}/A_{RMS}$.

The product of T_dT_{50ex} was chosen here as it was proved to bring more information about potential tsunami generation by underwater earthquakes than other discriminants do, for example, the moment magnitude M_w. As pointed out by Necmioglu and Özel (2014), determination of rupture duration had a relatively large uncertainty affecting accurate prediction of tsunami initiation hence being improper for tsunami hazard assessment. A similar situation to occur was found for earthquake magnitude, scaled with any measurement, as the earthquake magnitude was proved to be inaccurate for tsunami analysis and assessment (Madlazim and Prastowo, 2016).

The product of $T_dT_{50ex} \geq 10$ s is then found to be a good discriminant for tsunami generation. We modify the procedures described in Lomax and Michelini (2011), including the minimum distance reduced to 5° for all measurements by applying M-filter to select good seismograms for calculating T_d and T_{50ex} for local to regional events (Madlazim et al., 2018).

3. Application to recent large earthquakes

A total of 51 events, covering varying magnitudes from $6.5 \leq M_w \leq 8.6$ during 2011-2020, and consisting of 19 strike-slips, 17 normal-faulting and 15 reverse-faulting mechanisms were examined in this study. These earthquakes were events with either continent-centered or ocean-centered epicenter (Table 1 see Appendix at end of this report). These events were analyzed using the tsunami discriminant in terms of T_dT_{50ex} values for potential tsunami generation. The data were acquired from real-time network of seismic stations on the basis of regional and teleseismic real time data provided by the German Research Centre for Geosciences, known as GEOFON GFZ, and the Incorporated Research Institutions for Seismology-Data Management Center (IRIS-DMC).

RESULTS AND DISCUSSIONS

The earthquake data selected in this study (Table 1) is limited to earthquakes that have the smallest moment magnitude (M_w) 6.5, due to earthquakes with M_w below threshold signal to noise ratio is too bad and false automatic recognition of the P wave onset (Clément, J. and Reymond, D., 2014) which can causes false discriminant measurement results and becomes inefficient. A strong determination of the first motion of the P wave is key this method. We used the automatic picker Filter Picker - a Robust method, Broadband Picker for Real-Time Seismic Monitoring and Earthquake Early Warning for picking P wave data (Lomax, A. et al., 2012).

For all earthquakes examined in this study, we estimated T_dT_{50ex} values and compared them with TEV. Estimates of T_d and T_{50ex} were performed using the direct procedures previously presented. Table 1, and Table 2 (see Appendix) explained that by using the T_dT_{50ex} discriminant, the accuracy of tsunami early warning was obtained in about 4 minutes after the OT (True warning = TW) was 76%. Meanwhile, by using the discriminant moment magnitude (M_w), the accuracy of

tsunami early warning was obtained in about 10 to 15 minutes after the OT (True warning = TW) was 71%. The rupture duration measurement by using direct procedure is faster than the M_w measurement because the discriminant measurement used the direct procedure method of earthquake seismogram data, without going through an inversion (Lomax, A. & A. Michelini, 2012). How good the M_w discriminant is in correspond to TEV values. Here, we used the threshold value of $M_w \geq 7.0$ given by an earthquake of land-centered or sea-centered origin, corresponding to TEV ≥ 3 for tsunami generation.

The results for all the events examined in this study that T_dT_{50ex} values in the vertical axis for real-time application and evaluated at OT + 4 minutes, compared with TEV in the horizontal axis. The horizontal red solid-line and vertical red dashed line show the threshold value of T_dT_{50ex} and TEV, respectively. Triangles indicate tsunami occurrences and circles indicate no tsunami threats. Quadrant one is a zone where T_dT_{50ex} is equal to or greater than the threshold (10 seconds) and TEV is equal to or greater than 3. This means that in this zone an earthquake has the potential to cause a tsunami. Of the 37 tsunami events in zone three, the type of earthquake mechanism varies, not only revers, but there are also earthquakes with strike-slip and normal fault type mechanisms (Power et al., 2017; Ulrich et al., 2019). This shows that the strike-slip type earthquake and normal fault can generate tsunamis as long as the discriminant T_dT_{50ex} is equal to or greater than the threshold. Meanwhile, quadrant 3 is a zone where T_dT_{50ex} is less than the threshold (10 seconds) and TEV is less than 3. This means that in zone three an earthquake has no potential for a tsunami. Earthquakes that are in zones one and three in this article we call True Warning (TW). We call earthquakes in zones two and four in this article False Warning (FW) as shown in Fig.2.

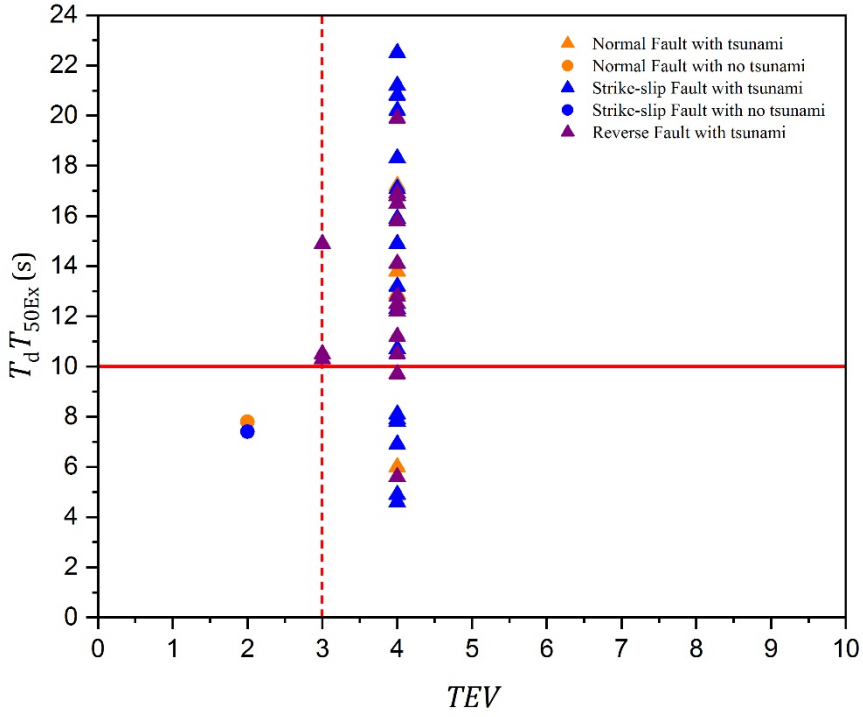

Figure 2. The results for all the events examined in this study. The T_dT_{50ex} values in the vertical axis for real-time application and evaluated at OT+4 minutes, compared with tsunami importance TEV in the horizontal axis. The horizontal red solid-line and vertical red dashed-line shows the threshold value of T_dT_{50ex} and TEV, resepectively. Triangles indicate tsunami occurrences and circles indicate no tsunami threats.

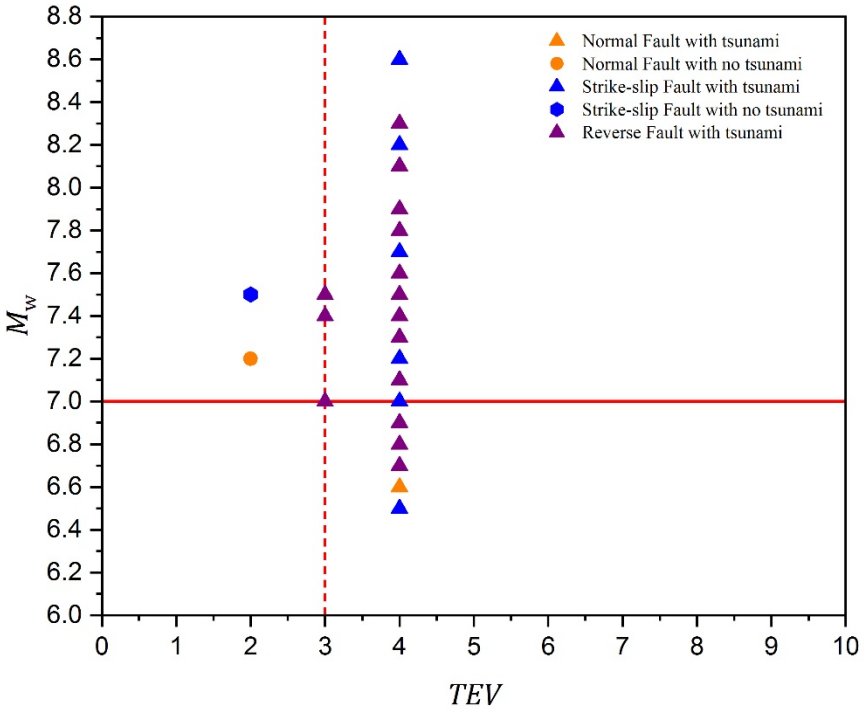

Figure 3. The results for all the events examined in this study. The $M_w$values in the vertical axis for real-time application and evaluated at OT + 15 minutes, compared with TEV in the horizontal axis.. The horizontal red solid-line and the vertical red dashed-line show the threshold value of M_w and TEV, respectively. Triangles indicate tsunami occurrences and circles indicate no tsunami threats.

The number of earthquakes occurring in the True Warning (TW) zone using the discriminant moment magnitude, M_w (Fig. 3) was less than that using the T_dT_{50ex} discriminant (Fig. 2). Meanwhile, the number of earthquakes occurred in the False Warning (FW) zone using the discriminant moment magnitude (M_w) in Fig. 3 is mostly compared to those using the T_dT_{50ex} discriminant (Fig. 2). This can be explained by the fact that M_w is a good discriminant for tsunami potential but it does not hold for all events having the potency for tsunami generation. In particular, the M_w discriminant does not work for slow‘tsunami earthquakes, which induce waves larger than would be expected from their sizes (Satake, 2002; Polet and Kanamori, 2009; Newman et al., 2011; Lomax, A and Michelini, A., 2012).

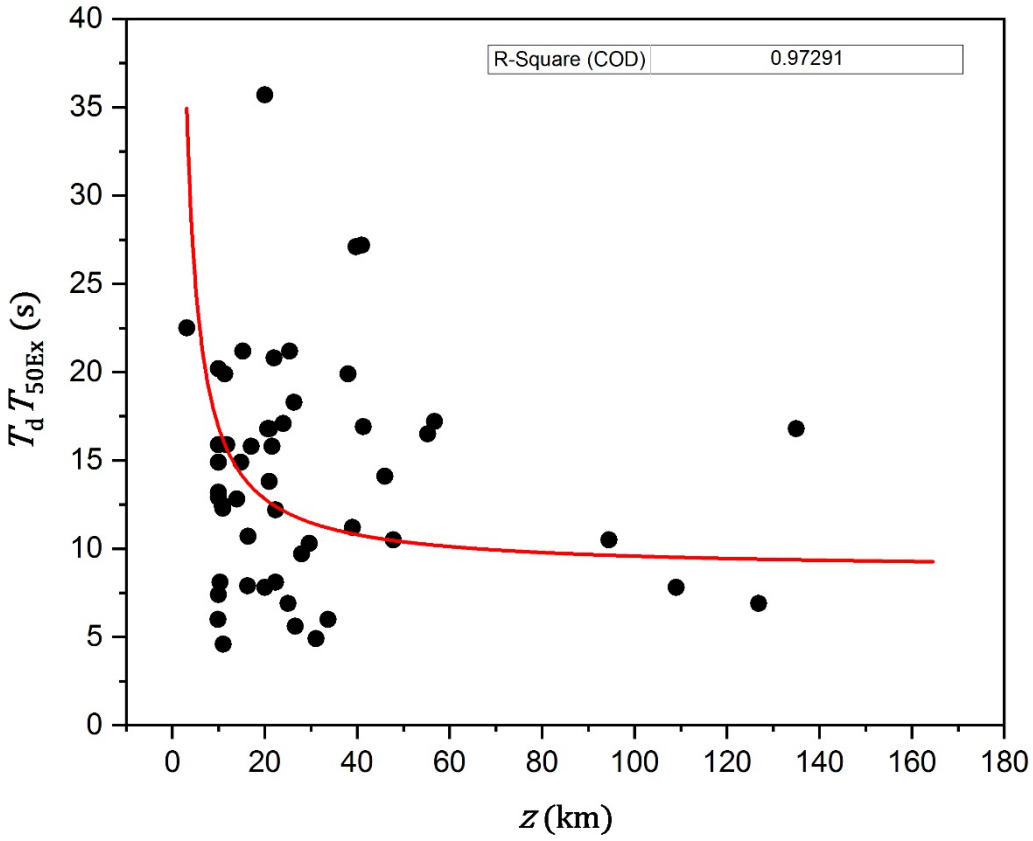

Figure 4. Relation between T_dT_{50ex} values for all the events and source depths, where the red line is exponential curve-fitting for the data distribution with a determination coefficient of 0.97.

For a T_dT_{50ex} value greater than or equal to 10 seconds, the depth of the earthquake source is less than or equal to 60 km. T_dT_{50ex} discriminant not only provides information about the existence of vertical displacement of the earthquake, however, provides information about the depth of the earthquake source (Lomax, A. & Mechelini, A., 2009). In the tsunami faulting model, the rupture length, L is proportional to the rupture duration or T50Ex which can be expressed in terms of T50Ex is proportional to L / v_r, where v_r is the rupture speed of the earthquake. Since v_r corresponds to the S wave velocity and shear modulus, μ, which increases with depth, and because v_r is found to be very low at shallow depths for some earthquakes (Geist and Bilek 2001; Polet and Kanamori 2009), we can assume $v_r \propto z^q$, where z is the multiple mean rupture depths and q is positive. Then, rupture duration is proportional to L / z^q, indicating that rupture duration provides information about L and z, and most importantly, rupture duration grows with increasing L and decreasing z, two conditions for increasing tsunami potential.

The findings provide insight into a possibility that the tsunami potential is possibly induced by an earthquake either continent-centered or ocean-centered and is independent of source mechanisms. For example, a large tsunami wave was generated by a strike-slip event that hit Kaikoura region in New Zealand on 13 November 2016 (Power *et al*., 2017; Ulrich *et al*., 2019) although a large tsunami wave induced by this type of earthquake is rare. Strike-slip earthquakes commonly produce small tsunamis in size because vertical displacement of rupture is not strong

enough to lift a huge amount of seawater (Ulrich *et al*., 2019). Meanwhile, for normal-faulting earthquakes, the rock layers from the hanging-wall drop down and the corresponding oscillatory force is relatively small to displace them back vertically. This mechanism is different from that induced by reverse-faulting earthquakes, where the rocks from the hanging-wall directly displace seawater upward.

CONCLUSIONS

Calculation of the T_dT_{50ex} discriminant is also completed almost four times quicker than that of the M_w scale, making it better for rapid assessment of tsunami hazard analysis. The results indicate that the potency for tsunami excitation weakly correlates to the LWD, derived from the seismic model (Lomax and Michelini, 2011; 2012), which reflects the earthquake size in terms of the M_w scale. These indicate that the T_dT_{50ex} discriminant, derived from tsunami tsunami faulting model, is quicker and more accurate than the M_w, obtained from seismic parameter, for effective tsunami early warning.

We have examined tsunami discriminant T_dT_{50ex} and validated them with TEV. We have also introduced a real-time, rapid assessment of tsunami potential using the T_dT_{50ex} discriminant, instead of M_w, which is filtered by the M-filter to select earthquake signals coming from the local and regional station to allow initial estimates of all tsunami parameters. We found that T_dT_{50ex} values provide more information on tsunami impact,source depth,, and size than M_w and other currently used discriminants do. The T_dT_{50ex} discriminant is sensitive to rupture length L and depth z, which control the vertical seafloor displacement and hence the potency for tsunami excitation. This discriminant can be obtained within 4 minutes after the origin time with real-time earthquake data available for most tsunami prone areas.

ACKNOWLEDGEMENTS

The authors would sincerely like to thank the Indonesian Agency for Geophysics, Climatology, and Meteorology (BMKG) for providing earthquake data used in this study. We also firmly acknowledge GEOFON GFZ and Incorporated Research Institutions for Seismology (IRIS) for which seismic data were freely available at http://eida.gfz-potsdam.de/webdc3/ and http://www.iris.edu/wilber3/find. This article has also benefited from constructive reviews from two anonymous reviewers. This work is funded by DRPM, The Ministry of Education and Culture, The Republic of Indonesia.

DATA AVAILABILITY STATEMENT (DAS)

We are happy to report the availability of data related to the results of our study as we write in this article. With this data accessibility information, we anticipate even more uses of this open data. The data analyzed in this study are available in the following urls: 1. T_dT_{50ex} data derived from public domain resources (our product). These data were derived from the following resources availablei n the public domain (our product) http://prediksi-tsunami.unesa.ac.id/www/history_event.html or http://prediksi-tsunami.unesa.ac.id/www/ 2).Tsunami Event Validity (TEV) data derived from public domain resources. These data were derived from the following resources available in the

public domain: https://www.ngdc.noaa.gov/hazel/view/hazards/tsunami/event-search 3).Moment magnitude (M_w) and earthquake parameters data derived from public domain resources. These data were derived from the following resources available in the public domain: https://ds.iris.edu/wilber3/find_event and http://prediksi-tsunami.unesa.ac.id/www/

REFERENCES

Clément, J. and Reymond, D., 2014 New Tsunami Forecast Tools for the French Polynesia Tsunami Warning System. *Pure and Applied Geophysics* 172(3-4). DOI: 10.1007/s00024-014-0888-6

Geist, E. L. & Bilek, S. L., 2001. Effect of depth-dependent shear modulus on tsunami generation along subduction zones, *Geophys. Res. Lett.*, **28**(7), 1315-1318.

Lay, T., Ye, L., Bai, Y., Cheung, K. F., Kanamori, H., Freymueller, J., Steblov. G. M. & Kogan, M. G., 2017. Rupture along 400 km of the Bering fracture zone in the Komandorsky islands earthquake (M_w 7.8) of 17 July 2017, *Geophys. Res. Lett.*, **44**(12), 12161-12169.

Lomax, A. & Michelini, A., 2009. Tsunami early warning using earthquake rupture duration, *Geophys. Res. Lett.*, **36**, L09306.

Lomax, A. & Michelini, A., 2011. Tsunami early warning using earthquake rupture duration and *P*-wave dominant period: the importance of length and depth of faulting, *Geophys. J. Int.*, **185**(1), 283-291.

Lomax, A. & Michelini, A., 2012. Tsunami early warning within five minutes, *Pure Appl. Geophys.,* **170**, 1385-1395.

Lomax, A., Satriano, C, and Vassallo, M., 2012. Automatic Picker Developments and Optimization: FilterPicker a Robust, Broadband Picker for Real-Time Seismic Monitoring and Earthquake Early Warning. *Seismological Research Letters* 83:531-540.

Madlazim, 2011. Toward Indonesian tsunami early warning system by using rapid rupture durations calculation, *Sci. Tsu. Hazards*, **30**(4), 233-243.

Madlazim, 2013. Assessment of tsunami generation potential through rapid analysis of seismic parameters-case study: comparison of the Sumatra earthquakes of 6 April and 25 October 2010, *Sci. Tsu. Hazards*, **32**(1), 29-38.

Madlazim, 2015. Validation of Joko Tingkir software using tsunami importance, *Sci. Tsu. Hazards*, **34**(3), 289-198.

Madlazim & Prastowo, T., 2016. Evaluation of earthquake parameters used in the Indonesian Tsunami Early Warning System, *Earthq. Sci.*, **29**(1), 27-33.

Madlazim, Prastowo, T., Rohadi, S. & Hardy, T., 2018. Filter-M application for automatic computation of P-wave dominant periods for tsunami early warning, *Sci. Tsu. Hazards*, **37**(1), 26-33.

Madlazim, Rohadi, S., Koesoema, S. & Meilianda, E., 2019. Development of tsunami early warning application four minutes after an earthquake, *Sci. Tsu. Hazards*, **38**(3), 132-141.

Nakamura, Y., 1988. On the urgent earthquake detection and alarm system (UrEDAS), *Proc. of the 9th World Conference on Earthquake Engineering*, Tokyo-Kyoto, Japan.

Necmioglu, Ö. & Özel, N. M., 2014. An earthquake source sensitivity analysis for tsunami propagation in the eastern Mediterranean, *Oceanog.*, **27**(2), 76-85.

Newman, A.V., Hayes, G., Wei, Y. & Convers, J., 2011. The 25 October 2010 Mentawai tsunami earthquake, from real-time discriminants, finite-fault rupture, and tsunami excitation, *Geophys. Res. Lett.*, **38**, L05302.

Polet, J. & Kanamori, H., 2009. Tsunami Earthquakes, in Encyclopedia of Complexity and Systems Science, edited by A. Meyers, Springer, New York, pp. 10370.

Power, W., Clark, K., King, D. N., Borrero, J., Howarth, J. & Lane, E. M., 2017. Tsunami runup and tide-gauge observations from the 14 november 2016 M7.8 Kaikoura earthquake, New Zealand. *Pure Appl*. *Geophys*., **174**(7), 2457-2473.

Satake, K., 1994. Mechanism of the 1992 Nicaragua tsunami earthquake. *Geophys*. *Res*. *Lett*., **21**(23), 2519-2522.

Satake, K., 2002. *Tsunamis*, in International Handbook of Earthquake and Engineering Seismology, pp. 437–451, eds W.H.K. Lee, H. Kanamori, P.C. Jennings & C. Kisslinger, Academic Press, Amsterdam.

Sutton, J., Vos, S. C., Wood, M. M. & Turner, M., 2018. Designing effective tsunami messages: examining the role of short messages and fear in warning response, *Weath., Clim., and Soc.,* **10**(1), 75-78.

Tsushima, H., Hirata, K., Hayashi, Y., Tanioka, Y., Kimura, K., Sakai, S., Shinohara, M., Kanazawa, T., Hino, R. & Maeda, K., 2011. Near‐field tsunami forecasting using offshore tsunami data from the 2011 off the Pacific coast of Tohoku Earthquake*, Earth, Plan. And Space.*, **63**, 821-826.

Ulrich, T., Vater, S., Madden, E. H., Behrens, J., van Dinther, Y., van Zelst, I., Fielding, E. J., Liang, C. & Gabriel, A. A., 2019. Coupled, physics-based modeling reveals earthquake displacements are critical to the 2018 Palu, Sulawesi Tsunami, *Pure Appl*. *Geophys*., **176**(32), 4069-4109.

Wu, Y. M. & Kanamori, H., 2005. Experiment on an onsite early warning method for the Taiwan early warning system, *Bull. Seismol. Soc. Am.*, **95**(1), 347-353.

APPENDIX (Tables 1 and 2)

Table 1. The results for tsunami parameter estimates from all the strike-slip and normal-faulting earthquakes within a time period of 2011-2020.

No.	Origin Time (UTC)	Location	Latitude	Longitude	Depth (km)	M_w	T_d (s)	T_{50ex}	T_dT_{50ex} (s)	TEV	TCC	Event	Type	Status
1.	2011-07-06 19:03:18	Kermadec Island	29.3° S	176.2° W	25.4	7.6	10.2	2.1	21.2	4	1	Yes	ONF	TW
2.	2012-03-09 07:09:53	Vanuatu Island	19.2° S	169.8° E	33.7	6.6	6.7	0.9	6.0	4	1	Yes	ONF	FW
3.	2012-04-11 08:38:37	Off West Coast of North Sumatra	2.2° N	93.0° E	26.3	8.6	9.4	2.0	18.3	4	1	Yes	OSSF	TW
4.	2012-04-11 10:43:10	Off West Coast of North Sumatra	0.8° N	92.4° E	21.6	8.2	7.8	2.0	15.8	4	1	Yes	OSSF	TW
5.	2013-01-05 08:58:19	Southeastern Alaska	55.2° N	134.8° W	3.1	7.5	14.1	1.6	22.5	4	1	Yes	OSSF	TW
6.	2013-02-28 15-26-38	Santa Cruz Island	10.9° S	166.2° E	22.4	7.0	4.9	1.7	8.1	4	1	Yes	OSSF	FW
7.	2013-07-21 05:09:32	Cook Strait	41.7° S	174.4° E	16.3	6.5	8.2	0.9	7.9	4	1	Yes	OSSF	FW
8.	2013-04-19 03:05:52	Kuril Island	46.1° N	150.9° E	109.0	7.2	2.9	2.8	7.8	2	1	No	ONF	TW
9.	2014-04-01 23:46:47	Near Coast Of Northern Chile	19.6° S	70.9° W	17.1	8.1	7.1	2.2	15.8	4	1	Yes	ORF	TW
10.	2014-04-12 20:14:38	Solomon Islands	11.2° S	162.1° W	15.3	7.6	11.7	1.8	21.2	4	1	Yes	OSSF	TW
11.	2014-04-19 13:28:00	Solomon Island	6.7° S	154.9° E	39.8	7.5	12.5	2.1	27.1	4	1	Yes	ORF	TW
12.	2014-11-15 02:31:42	Northern Molucca Sea	1.8° N	126.5° E	47.8	7.0	4.5	2.3	10.5	3	1	Yes	ORF	TW
13.	2015-02-16 23:06:28	Off East Coast Of Honshu	39.9° N	143.1° E	10.8	6.7	5.4	2.3	12.5	4	1	Yes	ORF	TW
14.	2015-03-29 23:48:31	New Britain Region	4.8° S	152.6° E	41.3	7.5	10.2	1.7	16.9	4	1	Yes	ORF	TW

15.	2015-05-05 01:44:04	New Britain Region	5.5° S	151.9° E	29.6	7.5	5.2	2.0	10.3	3	1	Yes	CRF	TW
16.	2015-07-10 04:12:42	Solomon Island	9.4° S	158.3° E	20.0	6.7	7.2	1.1	7.8	4	1	Yes	OSSF	FW
17.	2015-07-18 02:27:32	Santa Cruz Island	10.5° S	165.1° E	11.8	6.9	9.3	1.7	15.9	4	1	Yes	ONF	TW
18.	2015-09-16 22:54:32	Near Coast Of Central Chile	31.6° S	71.7° W	22.4	8.3	5.1	2.4	12.2	4	1	Yes	ORF	TW

No.	Origin Time (UTC)	Location	Latitude	Longitude	Depth (km)	M_w	T_d (s)	T_{50ex}	T_dT_{50ex} (s)	TEV	TCC	Event	Type	Status
19.	2015-11-17 07:10:07	Greece	38.7° N	20.6° E	11.0	6.5	2.5	1.0	4.6	4	3	Yes	CSSF	FW
20.	2016-03-02 12:49:48	Southwest of Sumatra	4.9° S	94.3° E	24.0	7.8	8.4	2.05	17.1	4	1	Yes	OSSF	TW
21..	2016-04-16 23:58:36	Near Coast Of Ecuador	0.4° N	79.9° W	20.6	7.8	9.4	1.8	16.8	4	1	Yes	CRF	TW
22.	2016-08-12 01:26:36	Southeast of Loyalty Island	22.5° S	173.1° E	16.4	7.2	9.4	1.1	10.7	4	1	Yes	OSSF	TW
23.	2016-08-1 07:32:22	South Georgia Island Region	55.3° S	31.9° W	10.0	7.4	10.0	1.5	14.9	3	1	Yes	ORF	TW
24.	2016-11-1 11:02:59	Kaikoura New Zealand	42.7° S	173.1° E	22.0	7.8	11.0	1.9	20.8	4	1	Yes	CSSF	TW
25.	2016-11-21 20:59:49	Near East Coast of Honsu	37.4° N	141.4° E	11.4	6.9	8.8	2.3	19.9	4	1	Yes	ONF	TW
26.	2016-11-24 18:43:48	Off Coast Of Central America	11.9° N	88.8° W	10.3	6.9	7.4	1.0	8.1	4	1	Yes	ONF	FW
27.	2016-12-08 17:38:46	Solomon Island	10.7° S	161.3° W	41.0	7.8	12.5	2.2	27.2	4	1	Yes	ORF	TW
28.	2016-12-09 19:10:07	Solomon Island	10.7° S	161.1° W	21.1	6.9	12.5	1.4	16.8	4	1	Yes	ORF	TW
29.	2016-12-17 10:51:10	New Ireland Region	4.5° S	153.5° E	94.5	7.9	5.6	1.9	10.5	4	1	Yes	ORF	TW
30.	2016-12-25 14:22:27	Southern Chile	43.4° S	73.9° W	38.0	7.6	9.0	2.2	19.9	4	1	Yes	ORF	TW

31.	2017-01-03 21:52:30	South of Fiji Island	19.4° S	176.1° E	126.9	6.9	9.5	0.7	6.9	4	1	Yes	ONF	FW
32.	2017-01-2 04:30:22	Solomon Islands	6.2° S	155.1° E	135.0	7.9	9.5	1.8	16.8	4	1	Yes	ORF	TW
33.	2017-07-17 23:34:13	Komandorskiye Ostrova	54.5° N	168.8° E	10.9	7.7	7.6	1.6	12.3	4	1	Yes	OSSF	TW
34.	2017-09-08 04:49:20	Near Coast of Chiapas Mexico	15.0° N	93.9° W	56.7	8.1	7.2	2.4	17.2	4	1	Yes	ONF	TW
35.	2017-11-01 02:23:55	Loyalty Islands	21.7° S	168.9° E	9.9	6.6	6.3	0.9	6.0	4	1	Yes	ONF	FW
36.	2018-01-10 02:51:31	North of Honduras	17.5° N	83.5° W	10.0	7.5	11.1	1.8	20.2	4	1	Yes	OSSF	TW

No.	Origin Time (UTC)	Location	Latitude	Longitude	Depth (km)	M_w	T_d (s)	T_{50ex}	T_dT_{50ex} (s)	TEV	TCC	Event	Type	Status
37.	2018-01-14 09:18:45	Near Coast Of Peru	15.8° S	74.7° W	39.0	7.1	7.5	1.5	11.2	4	1	Yes	ORF	TW
38.	2018-01-23 09:31:42	Gulf of Alaska	56.0° N	149.0° W	25.0	7.9	2.7	2.6	6.9	4	1	Yes	OSSF	FW
39.	2018-09-28 10:02:43	Palu Indonesia	0.2° S	119.8° E	10.0	7.5	8.4	1.9	15.9	4	3	Yes	CSSF	TW
40.	2018-08-29 03:51:56	Southeast Of Loyalty Islands	22.1° S	170.0° E	26.6	7.1	6.3	0.9	5.6	4	1	Yes	ORF	FW
41.	2018-10-25 22:54:52	Ionian Sea	37.5° N	20.6° E	14.0	6.8	5.3	2.4	12.8	4	1	Yes	ORF	TW
42.	2018-12-05 04:18:08	Southeast of Loyalty Island	21.9° S	169.4° E	10.0	7.5	8.6	1.5	12.9	4	1	Yes	ONF	TW
43.	2019-05-14 12:58:26	New Britain Region	4.1° S	152.6° E	10.0	7.5	8.6	0.8	7.4	2	1	No	OSSF	TW
44.	2019-06-15 22:55:04	Karmades Island	30.6° S	178.1° W	46.0	7.3	12.4	1.1	14.1	4	1	Yes	ORF	TW
45.	2020-01-28 19:10:24	Cuba Region	19.4° N	78.8° W	14.8	7.7	8.8	1.7	14.9	4	1	Yes	OSSF	TW

46.	2020-03-25 02:49:20	East Of Kuril Islands	48.9° N	157.7° E	55.3	7.5	8.3	2.0	16.5	4	1	Yes	ORF	TW
47.	2020-06-18 15:29:04	South Of Kermadec Islands	33.3° S	117.8° W	10.0	7.4	6.8	1.9	13.2	1	1	Yes	OSSF	TW
48.	2020-06-23 12:49:53	Near Coast Of Oaxaca, Mexico	15.9° N	96.0° W	20.0	7.4	18.9	1.9	35.7	4	1	Yes	CRF	TW
49.	2020-07-22 06:12:44	Alaska Peninsula	55.0° N	158.5° W	28.0	7.8	4.2	2.3	9.7	4	1	Yes	ORF	FW
50.	2020-10-19 20:54:39	South Of Alaska	54.6° N	159.6° W	31.1	7.6	2.3	2.2	4.9	4	1	Yes	OSSF	FW
51.	2020-10-30 11:51:27	Dodecanese Islands, Greece	37.1° N	26.8° E	21.0	7.0	8.6	1.6	13.8	4	1	Yes	ONF	TW

Notes: CSSF (Continental Strike-Slip Fault), OSSF (Oceanic Strike-Slip Fault), CNF (Continental Normal Fault), ONF (Oceanic Normal Fault), CRF (Continental Reverse Fault), ORF (Oceanic Reverse Fault), FW (False Warning), TW (True Warning), TEV (Tsunami Event Validity), TCC (Tsunami Cause Code)

Table 2. The results for assessment of tsunami potential using M_w and $T_d T_{50ex}$ discriminants.

Discriminant	Available (minutes after OT)	Threshold Value	True Warning (TW)			False warning (FW)		
			$TEV \geq 3$	$TEV < 3$	%**	$TEV \geq 3$	$TEV < 3$	%**
M_w	15	7.0	36	0	71%	13	2	29%
$T_d T_{50ex}$	4	10.0 s	39	2	76%	12	0	24%

*51 events classified; 39 occurrences have $TEV \geq 3$

** percentage of True Warning or False Warning